Effects of Dipolar Interaction on Spin–Orbit Coupled Dynamics in Spin-1 Ultracold Atoms

Qiang Zhao*

Department of Applied Physics, North, China University of Science and Technology, Tangshan 063210, China

In this paper, we investigate the spin–orbit coupling of $F = 1$ dipolar Bose–Einstein condensates in a quasi-one-dimensional trap by solving the mean field Gross–Pitaevskii equation. We focus on the two phases, ferromagnetic and antiferromagnetic. For the former, we find that the spin echo signal emerges gradually as the spin–orbit coupling strength increases, which favors miscibility in density profile. The dipolar interaction plays a tiny role in the spin dynamics process, the qualitative behavior remains almost unchanged. Nevertheless, for the antiferromagnetic phase, the physical picture greatly changes. The spin echo signal abruptly increases with the increase in spin–orbit coupling strength, and the density structure exhibits phase separation. With the emergence of dipolar interaction, the spin echo signal vanishes, and the evolution of the three components is ruleless. Meanwhile, the condensate deviates from the property of phase separation. Also, we analyze the effect of the number of atoms on spin dynamics. It is obvious that the reduction of atoms increases the number of spin echo signals for the ferromagnetic phase regardless of the nature of dipolar interaction. In addition, for the antiferromagnetic phase, such a decrease gives rise to the disappearance of the spin echo signal in the absence of dipolar interaction, and its influence is small when dipolar interaction is added.

topics: spin–orbit coupling, dipole–dipole interaction, phase separation, spin dynamics

1. Introduction

The recent realization of spin–orbit coupling (SOC) in ultracold neutral quantum gases opens a way for exploring nonlinear dynamics [1, 2] and topological phases [3, 4]. Many interesting physical phenomena related to SOC are investigated, such as the spin Hall effect [5, 6], topological insulators [7], collective excitations [8, 9], etc. Experimentally, SOC can be artificially introduced into Bose–Einstein condensates (BECs) using Raman lasers [10, 11]. Recently, the two-component [12, 13] and three-component [14] SOC BECs including the stripe, plane-wave, and zero-momentum phases have been successfully synthesized. Additionally, the dynamical instability is analyzed theoretically [15].

On the other hand, the experimental study of ultracold gases composed of high-magnetic-moment atoms has flourished. Unlike traditional BECs with only short-range contact interactions, the dipole–dipole interaction (DDI) plays an important role there. Many theoretical studies elaborate on the influence of DDI in different contexts, for example, quantum droplets [16, 17], super solids [18, 19], and stabilization of super-Tonks–Girardeau gases [20], among others [21, 22]. In particular, intense research is focused on the case of tilted dipoles. In [23], the authors explore the effect of the polarization direction on the dynamics of ring dark solitons. They find that the ring dark solitons evolve into an elliptical structure and then develop into vortex–antivortex pairs. In addition, the transition of density profile from miscible to immiscible mixture occurs as the tilting angles are varied [24]. For review characteristics of DDI in BECs, see [25] and references therein.

In recent years, the properties of dipolar condensate with SOC have been extensively studied. The plane-wave soliton and stripe soliton are investigated in binary BEC [26]; they possess spatially varying phases and spatially oscillating densities, respectively. Many topological structures, such as skyrmion with different topological charges, can be tuned [27]. Huang et al. demonstrate the possibility of stabilizing the excited states of semivortex and mixed-mode solitons [28]. In the work of Li et al. [29], the creation of gap solitons in free nearly two-dimensional space is reported, and the band gap spectrum is observed. Moreover, the families of two-dimensional composite solitons are discussed [30].

This work extends the discussion from the spin degree of freedom $F = 2$ system [31]. It is known that there are three phases in spin-2 BECs, i.e., ferromagnetic, antiferromagnetic, and cyclic phase. Here, we consider the spin dynamics of spin-1 dipolar BECs with SOC. For the $F = 1$ system, only ferromagnetic and antiferromagnetic phases exist. The respective typical atoms used in our calculation are ^{87}Rb and ^{23}Na. We aim to study how the DDI and SOC affect the physical properties of these two phases.

The layout of this paper is as follows. In Sect. 2, we present the theoretical model for quasi-one-dimensional (1D) three-component BECs. In Sect. 3, we give the main results of this paper, showing the effects of SOC and DDI on the time evolution of spin-exchange dynamics and spatial density structure. In particular, we analyze the influence of the number of atoms on these issues. Finally, Sect. 4 is devoted to summarizing remarks.

2. Theoretical model

We consider the trap potential harmonically confined along the y–z plane, i.e., $\omega_{yz} \gg \omega_x$. In this case, the radial motion of BEC is frozen. We assume that all the N atoms with mass M are in BEC described by the mean-field Gross–Pitaevskii (GP) equation [32, 33]

$$\mathrm{i}\frac{\partial \psi_1}{\partial t} = \left[-\frac{1}{2}\frac{\partial^2}{\partial x^2} + V(x) + c_0\rho + c_2(\rho_0 + \rho_1 - \rho_{-1})\right]\psi_1$$
$$+ c_2\psi_{-1}^*\psi_0^2 + c_d\mathcal{D}_z\psi_1 + c_d\mathcal{D}_-\psi_0 - \mathrm{i}\lambda\partial_x\psi_1,$$

$$\mathrm{i}\frac{\partial \psi_0}{\partial t} = \left[-\frac{1}{2}\frac{\partial^2}{\partial x^2} + V(x) + c_0\rho + c_2(\rho_1 + \rho_{-1})\right]\psi_0$$
$$+ 2c_2\psi_1\psi_{-1}\psi_0^* + c_d(\mathcal{D}_+\psi_1 + \mathcal{D}_-\psi_{-1})$$
$$- \mathrm{i}\lambda(\partial_x\psi_1 + \partial_x\psi_{-1}),$$

$$\mathrm{i}\frac{\partial \psi_{-1}}{\partial t} = \left[-\frac{1}{2}\frac{\partial^2}{\partial x^2} + V(x) + c_0\rho + c_2(\rho_0 - \rho_1 + \rho_{-1})\right]\psi_{-1}$$
$$+ c_2\psi_1^*\psi_0^2 - c_d\mathcal{D}_z\psi_{-1} + c_d\mathcal{D}_+\psi_0 - \mathrm{i}\lambda\partial_x\psi_{-1}, \quad (1)$$

where ψ_m ($m = 1, 0, -1$) is the three-components wavefunction with total density $\rho = \Sigma_m|\psi_m|^2$ and $V(x) = \frac{1}{2}x^2$. The population of the hyperfine state is $N_m = \int \mathrm{d}x \ |\psi_m(x)|^2$. The spin-independent and spin-dependent strengths are $c_0 = 4\pi N(a_0 + 2a_2)/(3M\omega_x l^3)$

and $c_2 = 4\pi N(a_2 - a_0)/(3\omega_x l^2)$, respectively, where a_0 (a_2) is s-wave scattering length in total spin $F = 0$ ($F = 2$), $l = \sqrt{\hbar/(M\omega_x)}$ is the oscillator length, and λ is the SOC strength. The dipole strength is $c_d = N\mu_0 Mg_F^2\mu_B^2/(4\pi l\hbar^2)$ with vacuum magnetic permeability μ_0, Bohr magneton μ_B, and Landé g-factor g_F. The dipole integral $\mathcal{D}_\nu = \int \mathrm{d}x' \ \Sigma_{\nu\nu'}P_{\nu\nu'}(x-x')S_{\nu'}(x')$ (with $\nu = x, y, z$) is treated by convolution theorem and $\mathcal{D}_\pm = (\mathcal{D}_x \pm \mathrm{i}\mathcal{D}_y)/\sqrt{2}$. The dipole kernel $P_{\nu\nu'}(x)$ in momentum space is [34]

$$\tilde{P}(k_x) = \frac{2\pi}{3}\left[1 - 3G\left(\frac{k_x\sqrt{w_x}}{\sqrt{w_{yz}}}\right)\right]\begin{pmatrix} 1 & 0 & 0 \\ 0 & 1 & 0 \\ 0 & 0 & 1 \end{pmatrix}, \quad (2)$$

where $G(x) = x^2\mathrm{e}^{x^2}\int_{x^2}^{\infty}\mathrm{d}t \ \frac{1}{t}\mathrm{e}^{-t}$ denotes the exponential function. The spin density is $S_\nu(x) = \Sigma_{m,m'=-1}^{1}(\boldsymbol{F}_\nu)_{mm'}\psi_m^\dagger\psi_{m'}$ with spin-1 matrices $\boldsymbol{F} = (F_x, F_y, F_z)$.

Numerically, we solve (1) without SOC and DDI to obtain the ground state via the imaginary time evolution approach. The normalization condition and magnetization are $\int_{-\infty}^{\infty}\mathrm{d}x \ \rho(x) = 1$ and $\mathcal{M} = \int_{-\infty}^{\infty}\mathrm{d}x \ [\rho_1(x) - \rho_{-1}(x)]$, respectively. To ensure the constant of magnetization $\mathcal{M}$ and normalization, the normalization coefficients of the three-components $m = 1, 0, -1$ are

$$d_0 = \frac{\sqrt{1 - \mathcal{M}^2}}{\sqrt{N_0 + \sqrt{4(1 - \mathcal{M}^2)N_1N_{-1} + \mathcal{M}^2N_0^2}}},$$

$$d_1 = \sqrt{\frac{1 + \mathcal{M} - d_0^2N_0}{2N_1}},$$

$$d_{-1} = \sqrt{\frac{1 - \mathcal{M} - d_0^2N_0}{2N_{-1}}}, \quad (3)$$

respectively. The real-time propagation with time splitting method [35] is then performed by evolving the ground state with the inclusion of the SOC and DDI, i.e., $\psi_m(t + \Delta t) = \hat{U}\psi_m(t)$, where the unitary propagator is $\hat{U} = \exp\left[-\mathrm{i}\Delta t(H_{\mathrm{KE}} + H_{\mathrm{SOC}} + H_{\mathrm{SE}} + H_{\mathrm{SP}})\right]$ with

$$H_{\mathrm{KE}} = -\frac{1}{2}\begin{pmatrix} \partial_{xx} & 0 & 0 \\ 0 & \partial_{xx} & 0 \\ 0 & 0 & \partial_{xx} \end{pmatrix}, \quad (4)$$

$$H_{\mathrm{SOC}} = -\mathrm{i}\lambda\begin{pmatrix} 0 & \partial_x & 0 \\ \partial_x & 0 & \partial_x \\ 0 & \partial_x & 0 \end{pmatrix}, \quad (5)$$

$$H_{\mathrm{SE}} = \begin{pmatrix} 0 & c_2\psi_0\psi_{-1}^* + c_d\mathcal{D}_- & 0 \\ c_2\psi_0^*\psi_{-1} + c_d\mathcal{D}_+ & 0 & c_2\psi_0^*\psi_1 + c_d\mathcal{D}_- \\ 0 & c_2\psi_0\psi_1^* + c_d\mathcal{D}_+ & 0 \end{pmatrix}, \quad (6)$$

$$H_{\mathrm{SP}} = \begin{pmatrix} V + c_0\rho + c_2(\rho_1 + \rho_0 - \rho_{-1}) + c_d\mathcal{D}_z & 0 & 0 \\ 0 & V + c_0\rho + c_2(\rho_1 + \rho_{-1}) & 0 \\ 0 & 0 & V + c_0\rho + c_2(\rho_0 + \rho_{-1} - \rho_1) - c_d\mathcal{D}_z \end{pmatrix}. \quad (7)$$

The spatial and time steps are $\Delta x = 0.011$ and $\Delta t = 0.001$, respectively.

3. Results and discussion

In this section, we first give the interaction strengths used in this manuscript. We consider $N = 10000$ atoms trapped in quasi-1D trap potential with $\omega_x = 2\pi \times 20$ Hz, and the aspect ratio $\gamma = \frac{\omega_{yz}}{\omega_x}$ is equal to 20. The scattering lengths a_0, a_2 for ferromagnetic ^{87}Rb and antiferromagnetic ^{23}Na are $101.8a_{\mathrm{B}}, 101.4a_{\mathrm{B}}$ [36] and $50.0a_{\mathrm{B}}, 55.01a_{\mathrm{B}}$ [37], where a_{B} is the Bohr radius. The Landé g-factor $g_F = 1/2$. Under this parameters condition, the dimensionless interaction strengths (c_0, c_2, c_d) for ^{87}Rb and ^{23}Na are $(885.0, -4.1, 0.37)$ and $(241.0, 7.5, 0.05)$, and $l = 4.69$ μm and $\omega_x^{-1} = 7.96 \times 10^{-3}$ s are the respective units of length and time employed in the manuscript. It is known that increasing dipole

strength can accelerate dipole dynamics, which allows one to observe the physical phenomena earlier [38]. Here, we adopt this scheme by increasing dipole strength by a factor of 30 to reach this purpose, i.e., new dipole strength $c_d' = 30c_d$.

We first analyze the spin dynamics for ^{87}Rb atoms without DDI, as shown in Fig. 1. The magnetization is fixed as $\mathcal{M} = 0.3$, and the curves drawn in dashed black, solid red, and dotted blue are for the components $m = 1, 0$, and -1, respectively. We mention that the same symbols of the three components are used in the rest of the manuscript. Overall, it is obvious that the alternant oscillation appears and the periodicity is the same between component $m = \pm 1$, and the spin dynamics of component $m = 1$ is opposite to component $m = -1$. In addition, the aperiodic oscillation of component $m = 0$ is confined to a small range. For Fig. 1a with $\lambda = 0.4$, the initial population N_1 decreases to a minimum at about $t_a = 30$. Then, it increases to a maximum at $t_b = 52$ for the first time. Next, N_1 decreases again and this process continuously
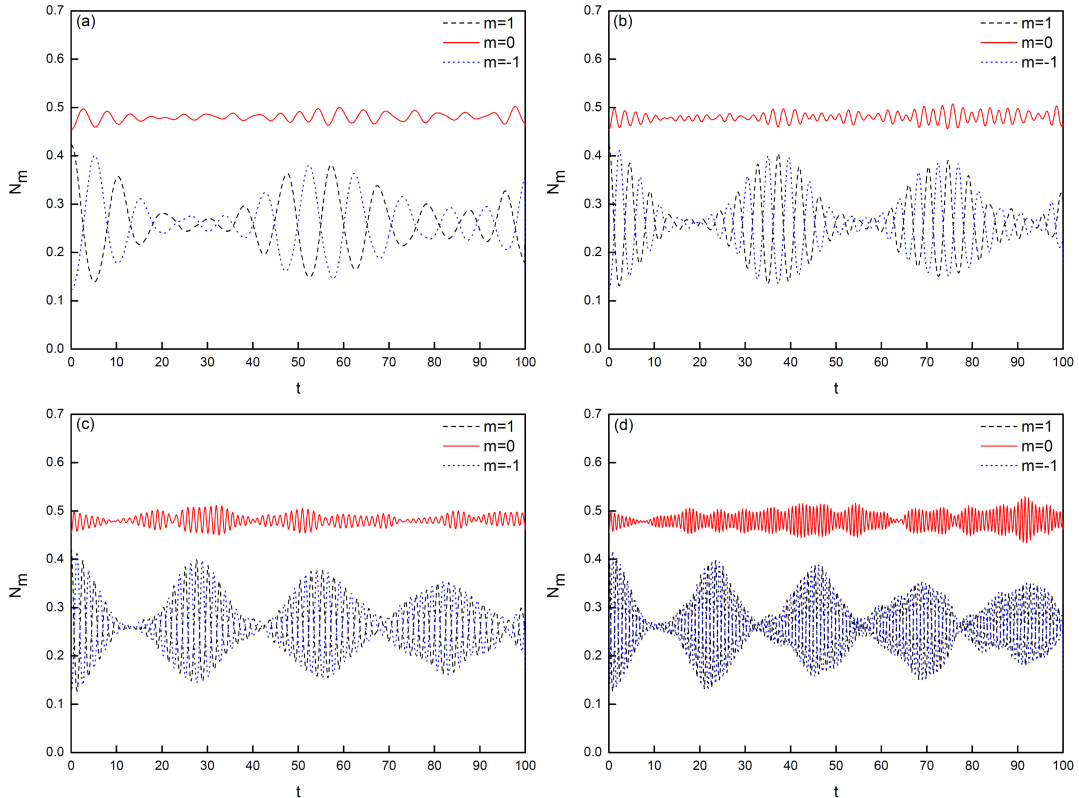

Fig. 1. Populations of spinor components with respect to time for ^{87}Rb atoms. The black, red, and blue lines correspond to $m = 1, 0$, and -1 states. The SOC strength $\lambda = 0.4, 0.6, 0.8$, and 1.0 for (a), (b), (c), and (d), respectively. Simulation parameters: $\mathcal{M} = 0.3$, $c_0 = 885.0$, and $c_2 = -4.1$.
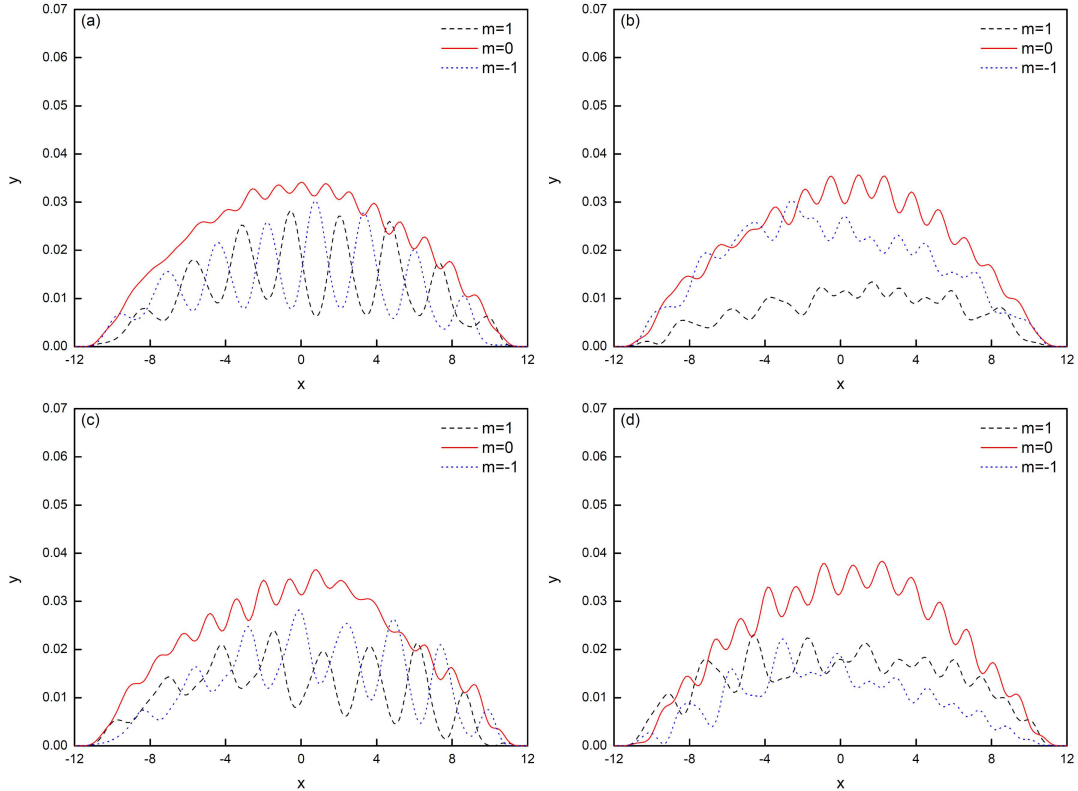
Fig. 2. Density profile for ^{87}Rb atoms at different moments: (a) $t = 20$, (b) $t = 40$, (c) $t = 60$, and (d) $t = 80$. The black, red, and blue lines correspond to $m = 1$, 0, and -1 states, respectively. Simulation parameters: $\mathcal{M} = 0.3$, $c_0 = 885.0$, $c_2 = -4.1$, and $\lambda = 0.6$.

proceeds. Here, we truncate the time evolution in $t = 100$. In fact, it is easy to envisage the existence of a second maximum and so on. For description, we call the curve of time evolution N_1 from time 0 to 30 the free induction decay (FID) signal and from time 30 to 52 the spin echo (SE) signal. Physically, FID and SE are discussed in magnetic resonance imaging. With the increase in SOC strength $\lambda = 0.6$ in Fig. 1b, the time t_a and t_b decrease, and the number of SE increases to 2. For larger $\lambda = 0.8$ in Fig. 1c and $\lambda = 1.0$ in Fig. 1d, one can see that t_a and t_b are further reduced and the number of SE becomes 3 and 4. For comparison, we list the values of t_a and t_b in Table I. Moreover, we note that the amplitude for the three components remains almost unchanged with the increase in SOC strength.

As an example, Fig. 2 displays the development of atom density at $\mathcal{M} = 0.3$ and $\lambda = 0.6$. It is remarkable that the density of component $m = 0$ is greater than component $m = \pm 1$ at the same space position, and the system presents a miscible configuration. In [32], the authors also show the miscible three-component density structure and argue that the configuration can be changed from immiscible to miscible by increasing $\mathcal{M}$. In our calculation, the magnetization $\mathcal{M}$ is fixed, and the immiscible configuration will be seen in the following discussions.

TABLE I

The approximate time t_a for the formation of FID and t_b for the first arrival of the maximum of SE at different SOC strengths λ. The parameters t_a, t_b and t_a', t_b' correspond to, respectively, $N = 10000$ and $N = 1000$ — the number of ^{87}Rb atoms. The magnetization $\mathcal{M} = 0.3$ in all the cases.

λ	t_a	t_a'	t_b	t_b'
0.4	30	17	52	30
0.6	20	10	38	19
0.8	10	8	28	15
1.0	8	5	24	12

In the case of the SOC antiferromagnetic condensate ^{23}Na, the physical picture changes greatly. Figure 3a and b presents the spin-exchange dynamics at SOC strength $\lambda = 0.4$ and 0.6, respectively. It is worth pointing out that: (i) there is no SE in $\lambda = 0.4$ and 0.5. The latter is verified in our simulation. To avoid repetition, the spin dynamics corresponding to $\lambda = 0.5$ is not given. (ii) The number of SE in $\lambda = 0.6$ is 8. It is important to emphasize that the SE is created abruptly, not gradually, as in the case of ^{87}Rb atoms. Furthermore, it is evident that the time spent on the creation of four
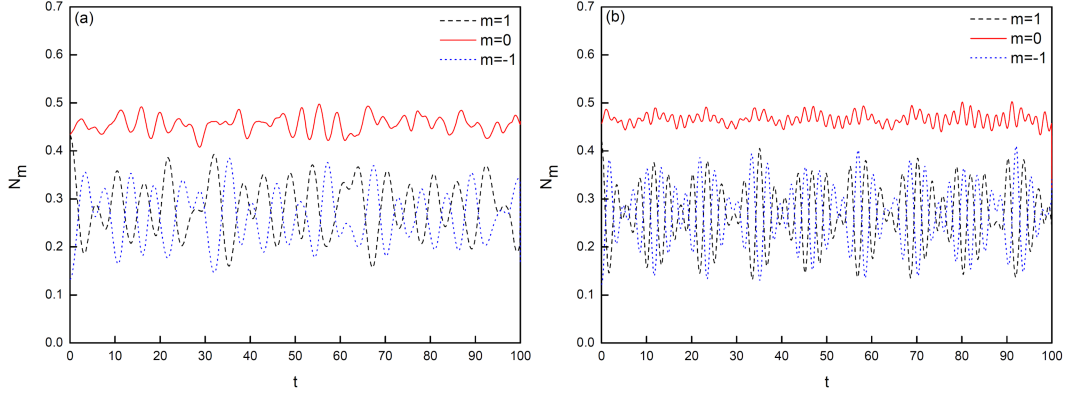
Fig. 3. Populations of spinor components with respect to time for ^{23}Na atoms. The black, red, and blue lines correspond to $m = 1$, 0, and -1 states, respectively. The SOC strength $\lambda = 0.4$ and 0.6 for (a) and (b). Simulation parameters: $\mathcal{M} = 0.3$, $c_0 = 241.0$, and $c_2 = 7.5$.
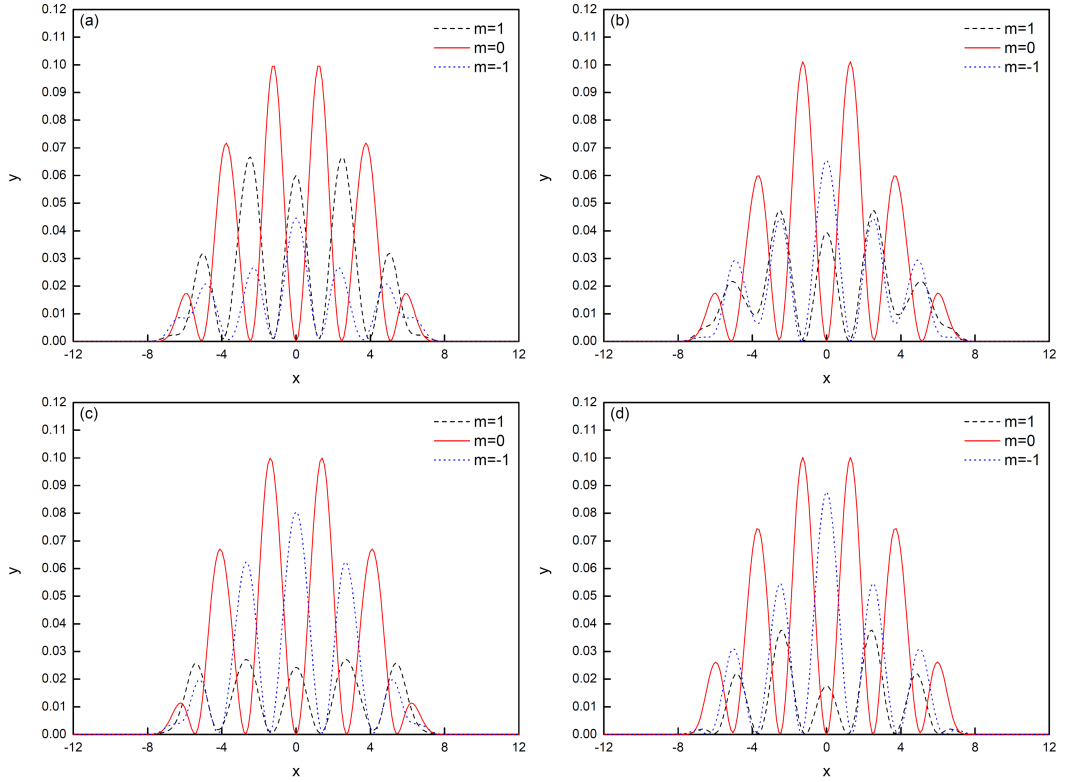

Fig. 4. Density profile for ^{23}Na atoms at different moments: (a) $t = 20$, (b) $t = 40$, (c) $t = 60$, and (d) $t = 80$. The black, red, and blue lines correspond to $m = 1$, 0, and -1 states, respectively. Simulation parameters: $\mathcal{M} = 0.3$, $c_0 = 241.0$, $c_2 = 7.5$, and $\lambda = 0.6$.

SE signals is about 50, which is much smaller than for ^{87}Rb atoms in Fig. 1d. In addition, we also plot the instant density profile. Figure 4 displays the numerical results at $\lambda = 0.6$. Compared to Fig. 2, the most obvious feature is the occurrence of phase separation. When the component $m = 0$ lies in the maximum density, the component $m = \pm 1$ is the minimum. In addition, the density difference between $m = 1$ and $m = -1$ weakens from the center $x = 0$ towards the peripheral of the condensate.

Next, we investigate the effect of DDI on the spin dynamics and density profile. Figure 5a shows the population of ^{87}Rb atoms at dipole strength $c_d' = 30c_d$ and SOC strength $\lambda = 0.6$. We find that the qualitative dynamics behavior and the time for the formation of FID and the first arrival of the maximum of SE coincide with Fig. 1b. The quantitative difference lies in the formation process of a SE signal. In the absence of DDI, the oscillation of the component $m = \pm 1$ is faster than in the
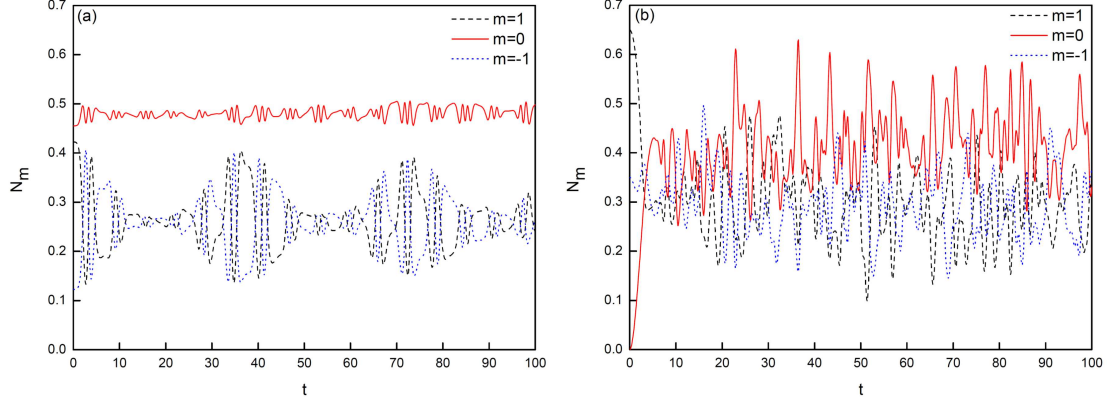
Fig. 5. Populations of spinor components with respect to time for (a) ^{87}Rb and (b) ^{23}Na atoms with DDI. The black, red, and blue lines correspond to $m = 1$, 0, and -1 states, respectively. The parameters c_0 and c_2 for (a) and (b) are 885.0, -4.1 and 241.0, 7.5, respectively. Simulation parameters: $\mathcal{M} = 0.3$, $\lambda = 0.6$, and $c_d' = 30c_d$.

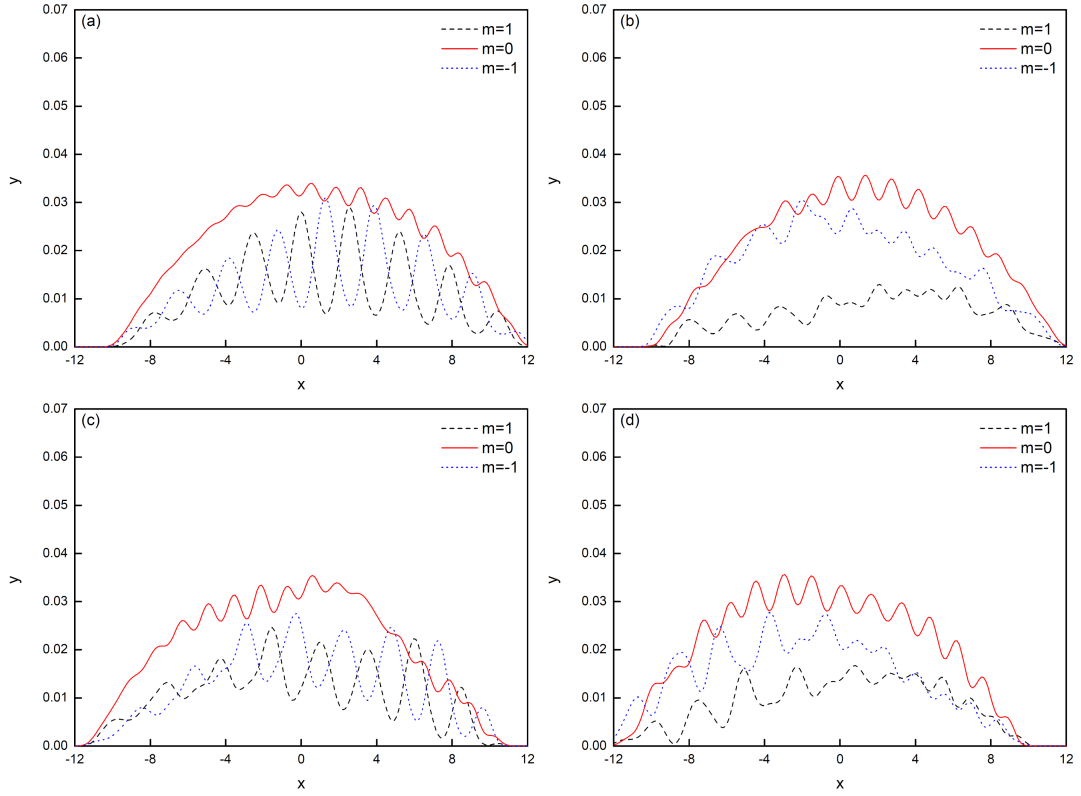Fig. 6. Density profile for ^{87}Rb atoms with DDI at different moments: (a) $t = 20$, (b) $t = 40$, (c) $t = 60$, and (d) $t = 80$. The black, red, and blue lines correspond to $m = 1$, 0, and -1 states, respectively. Simulation parameters: $\mathcal{M} = 0.3$, $c_0 = 885.0$, $c_2 = -4.1$, $\lambda = 0.6$, and $c_d' = 30c_d$.

presence of DDI. Meanwhile, we observe that the immiscible density configuration still holds, as shown in Fig. 6. It is noted that the dipole–dipole interactions greatly change the spin dynamics in SOC spin-2 ferromagnetic condensates such as ^{87}Rb atoms, indicating that the SE is broken and the three components individually reach steady population [31]. Nevertheless, the ^{23}Na atoms display

different properties in Fig. 5b when DDI is considered. The spin echo completely disappears, and the oscillation of the three components is irregular. Furthermore, the density profile in Fig. 7 shows that the characteristics of phase separation get worse.

It is also interesting to investigate the influence of the number of atoms on the spin dynamics. This issue is studied by Gautam [39], where the ground
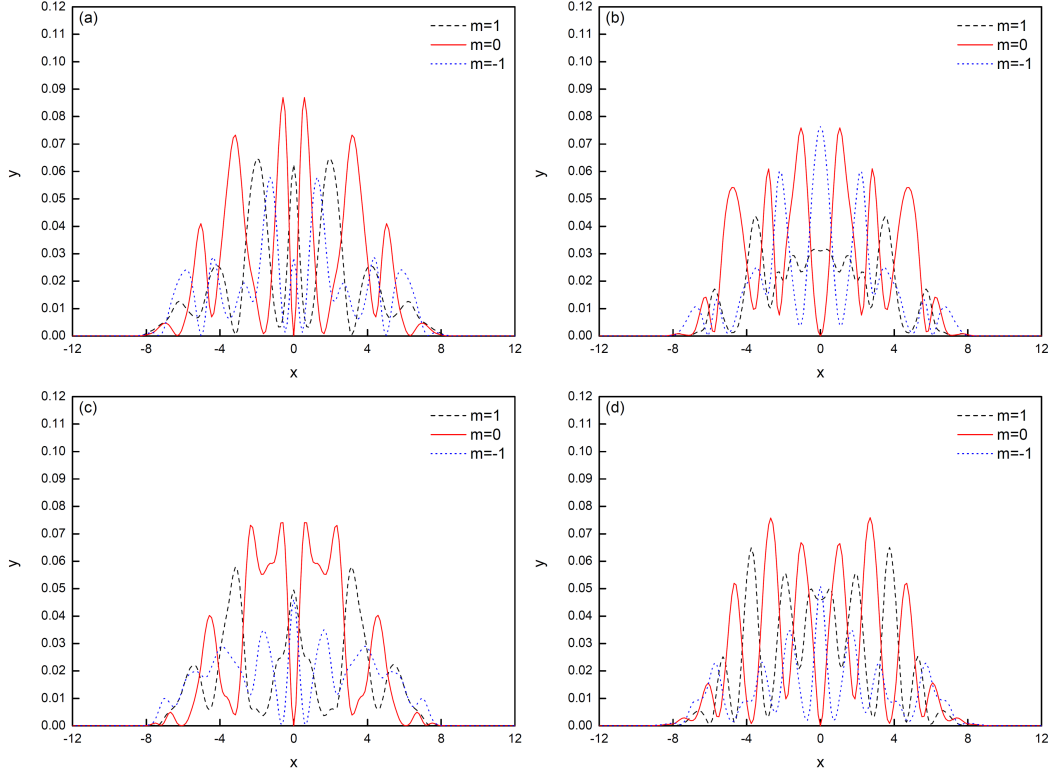
Fig. 7. Density profile for ^{23}Na atoms with DDI at different moments: (a) $t = 20$, (b) $t = 40$, (c) $t = 60$, and (d) $t = 80$. The black, red, and blue lines correspond to $m = 1$, 0, and -1 states, respectively. Simulation parameters: $\mathcal{M} = 0.3$, $c_0 = 241.0$, $c_2 = 7.5$, $\lambda = 0.6$, and $c'_d = 30c_d$.
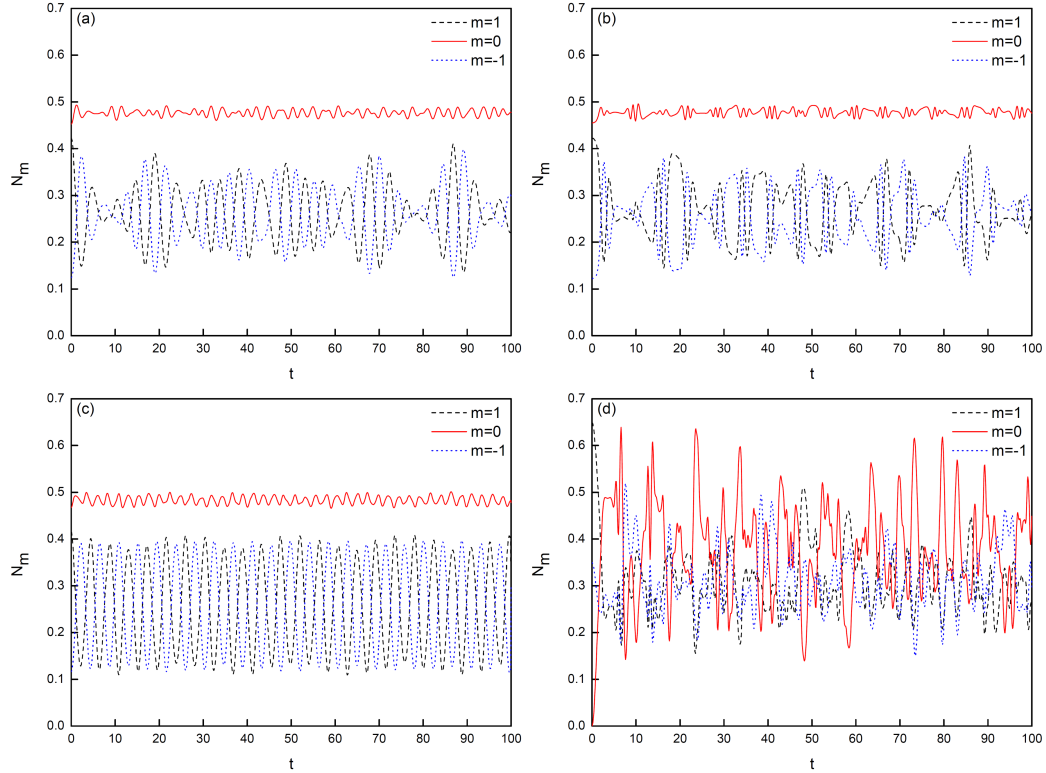

Fig. 8. Populations of spinor components with respect to time with 1000 atoms. The black, red, and blue lines correspond to $m = 1$, 0, and -1 states, respectively, for the system with (a) ^{87}Rb, (b) ^{87}Rb with DDI, (c) ^{23}Na, and (d)^{23}Na with DDI. Simulation parameters: $\mathcal{M} = 0.3$, $\lambda = 0.6$.

state of SOC spin-1 BEC in a quasi-1D potential is discussed. Here, we focus on the dynamics behavior and set $N = 1000$, which is 10 times less than the previous case. Figure 8 shows the populations of spinor components with respect to time. Four cases are analyzed: (a) ^{87}Rb, (b) ^{87}Rb with DDI, (c) ^{23}Na, (d) ^{23}Na with DDI. It is clear that for the cases in panels (a) and (b) compared with the cases in Fig. 1b and Fig. 3b the number of SE increases to 5. That is to say, the reduction of atoms helps create more SE in the ferromagnetic condensate. As a consequence, the time spent on the formation of SE decreases. Similarly, we also list the time t_a and t_b at different SOC strengths in Table I in order to differentiate the cases of $N = 10000$, which are expressed by t'_a and t'_b. In panel (c), there is no SE in the dynamics evolution, which is different from the results in Fig. 5a. This fact reflects that the reduction of atoms is unfavorable for SE generation in the antiferromagnetic phase. At last, the emergence of SE is still not seen in panel (d) with the existence of DDI. This point is consistent with the observation in Fig. 5b, which implies that the effect of the number of atoms on antiferromagnetic dipolar BECs is slight.

4. Conclusions

In conclusion, we study the spin dynamics of spin-1 dipolar BECs with SOC. For the ferromagnetic ^{87}Rb atoms, our results show that increasing SOC strength favors the gradual appearance of the SE signal, and the density profile for the three-component BECs is miscible. However, the scenario changes in antiferromagnetic ^{23}Na atoms. The number of SE suddenly increases with the increase in SOC strength, and the phase separation of space density appears. Moreover, the effect of DDI on spin dynamics for ^{87}Rb atoms is small, while it greatly affects the ^{23}Na atoms. As a result, the SE signal in ^{23}Na atoms disappears and the variation of the three components is irregular. Also, we find that the miscible configuration is still kept. However, the feature of phase separation gets worse. Finally, we also discuss the influence of the number of atoms on spin dynamics. It is seen that the decrease in the number of atoms makes the SE increase for the ferromagnetic phase with and without DDI. In addition, in the absence of DDI, such reduction leads to the absence of SE in the antiferromagnetic phase and, its effect is minor when DDI is considered.

Acknowledgments

References

[1] R.M. Kroeze, Y.D. Guo, B.L. Lev, *Phys. Rev. Lett.* **123**, 160404 (2019).

[2] K. Rajaswathi, S. Bhuvaneswari, R. Radha, P. Muruganandam, *Phys. Rev. A* **108**, 033317 (2023).

[3] N.R. Cooper, J. Dalibard, I.B. Spielman, *Rev. Mod. Phys.* **91**, 015005 (2019).

[4] D.W. Zhang, Y.Q. Zhu, Y.X. Zhao, H. Yan, S.L. Zhu, *Adv. Phys.* **67**, 253 (2018).

[5] M. Aidelsburger, M. Atala, M. Lohse, J.T. Barreiro, B. Paredes, I. Bloch, *Phys. Rev. Lett.* **111**, 185301 (2013).

[6] V. Galitski, I.B. Spielman, *Nature* **494**, 49 (2013).

[7] N. Goldman, I. Satija, P. Nikolic, A. Bermudez, M.A. MartinDelgado, M. Lewenstein, I.B. Spielman, *Phys. Rev. Lett.* **105**, 255302 (2010).

[8] Y.Y. Chen, H. Lyu, Y. Xu, Y.P. Zhang, *New J. Phys.* **24**, 073041 (2022).

[9] R. Ravisankar, H. Fabrelli, A. Gammal, P. Muruganandam, P.K. Mishra, *Phys. Rev. A* **104**, 053315 (2021).

[10] Y.J. Lin, R.L. Compton, A.R. Perry, W.D. Phillips, J.V. Porto, I.B. Spielman, *Phys. Rev. Lett.* **102**, 130401 (2009).

[11] Y.J. Lin, R.L. Compton, K. Jiménez-García, W.D. Phillips, J.V. Porto, I.B. Spielman, *Nat. Phys.* **7**, 531 (2011).

[12] Z. Wu, L. Zhang, W. Sun, X.T. Xu, B.Z. Wang, S.C. Ji, Y. Deng, S. Chen, X.J. Liu, J.W. Pan, *Science* **354**, 83 (2016).

[13] W. Sun, B.Z. Wang, X.T. Xu, C.R. Yi, L. Zhang, Z. Wu, Y. Deng, X.J. Liu, S. Chen, J.W. Pan, *Phys. Rev. Lett.* **121**, 150401 (2018).

[14] D.L. Campbell, R.M. Price, A. Putra, A. Valdés-Curiel, D. Trypogeorgos, I.B. Spielman, *Nat. Commun.* **7**, 10897 (2016).

[15] C. Hamner, Y. Zhang, M.A. Khamehchi, M.J. Davis, P. Engels, *Phys. Rev. Lett.* **114**, 070401 (2015).

[16] J.C. Smith, D. Baillie, P.B. Blakie, *Phys. Rev. Lett.* **126**, 025302 (2021).

[17] S. Pal, D. Baillie, P.B. Blakie, *Phys. Rev. A* **105**, 023308 (2022).

[18] A. Alaña, I.L. Egusquiza, M. Modugno, *Phys. Rev. A* **108**, 033316 (2023).

[19] G. Natale, R.M.W. van Bijnen, A. Patscheider, D. Petter, M.J. Mark, L. Chomaz, F. Ferlaino, *Phys. Rev. Lett.* **123**, 050402 (2019).

[20] W. Kao, K.Y. Li, K.Y. Lin, S. Gopalakrishnan, B.L. Lev, *Science* **371**, 296 (2021).

[21] M. Wenzel, F. Böttcher, T. Langen, I. Ferrier-Barbut, T. Pfau, *Phys. Rev. A* **96**, 053630 (2017).

[22] L. Klaus, T. Bland, E. Poli, C. Politi, G. Lamporesi, E. Casotti, R.N. Bisset, M.J. Mark, F. Ferlaino, *Nat. Phys.* **18**, 1453 (2022).

[23] G.Q. Yang, S.Y. Xie, Y. Zhao, J.J. Jin, S.Y. Zhang, *Physica A* **609**, 128398 (2023).

[24] A. Hocine, M. Benarous, *J. Low Temp. Phys.* **194**, 209 (2019).

[25] L. Chomaz, I. Ferrier-Barbut, F. Ferlaino, B. Laburthe-Tolra, B.L. Lev, T. Pfau, *Rep. Prog. Phys.* **86**, 026401 (2023).

[26] Y. Xu, Y.P. Zhang, C.W. Zhang, *Phys. Rev. A* **92**, 013633 (2015).

[27] B. Dong, S.L. Chen, X.F. Zhang, *Ann. Phys.* **447**, 169140 (2022).

[28] C.Q. Huang, Y.B. Ye, S.M. Liu, H.X. He, W. Pang, B.A. Malomed, Y.Y. Li, *Phys. Rev. A* **97**, 013636 (2018).

[29] Y.Y. Li, Y. Liu, Z.W. Fan, W. Pang, S.H. Fu, B.A. Malomed, *Phys. Rev. A* **95**, 063613 (2017).

[30] X.D. Jiang, Z.W. Fan, Z.P. Chen, W. Pang, Y.Y. Li, B.A. Malomed, *Phys. Rev. A* **93**, 023633 (2016).

[31] Q. Zhao, *Mod. Phys. Lett. B* **36**, 2250070 (2022).

[32] S. Gautam, S.K. Adhikari, *Phys. Rev. A* **90**, 043619 (2014).

[33] T. Świsłocki, T. Sowiński, J. Pietraszewicz, M. Brewczyk, M. Lewenstein, J. Zakrzewski, M. Gajda, *Phys. Rev. A* **83**, 063617 (2011).

[34] Y. Kawaguchi, M. Ueda, *Phys. Rep.* **520**, 253 (2012).

[35] P. Banger, P. Kaur, A. Roy, S. Gautam, *Comput. Phys. Commun.* **279**, 108442 (2022).

[36] E.G.M. van Kempen, S.J.J.M.F. Kokkelmans, D.J. Heinzen, B.J. Verhaar, *Phys. Rev. Lett.* **88**, 093201 (2002).

[37] A. Crubellier, O. Dulieu, F. Masnou-Seeuws, M. Elbs, H. Köckel, E. Tiemann, *Eur. Phys. J. D* **6**, 211 (1999).

[38] B.Y. Ning, S. Yi, J. Zhuang, J.Q. You, W.X. Zhang, *Phys. Rev. A* **85**, 053646 (2012).

[39] S. Gautam, S. K. Adhikari, *Phys. Rev. A* **90**, 043619 (2014).